

# Prospects for Observing High-redshift Radio-loud Quasars in the SKA Era: Paving the Way for 21-cm Forest Observations

QI NIU <sup>1</sup>, YICHAO LI <sup>1</sup>, YIDONG XU <sup>2,3</sup>, HONG GUO <sup>4</sup>, AND XIN ZHANG <sup>1,5,6</sup>

<sup>1</sup>Key Laboratory of Cosmology and Astrophysics (Liaoning) & College of Sciences, Northeastern University, Shenyang 110819, P. R. China

<sup>2</sup>National Astronomical Observatories, Chinese Academy of Sciences, Beijing 100101, China

<sup>3</sup>Key Laboratory of Radio Astronomy and Technology, Chinese Academy of Sciences, Beijing 100101, P. R. China

<sup>4</sup>Shanghai Astronomical Observatory, Chinese Academy of Sciences, Shanghai 200030, P. R. China

<sup>5</sup>National Frontiers Science Center for Industrial Intelligence and Systems Optimization, Northeastern University, Shenyang 110819, P. R. China

<sup>6</sup>Key Laboratory of Data Analytics and Optimization for Smart Industry (Ministry of Education), Northeastern University, Shenyang 110819, P. R. China

## ABSTRACT

The 21-cm forest is a sensitive probe for the early heating process and small-scale structures during the epoch of reionization (EoR), to be realized with the upcoming Square Kilometre Array (SKA). Its detection relies on the availability of radio-bright background sources, among which the radio-loud quasars are very promising, but their abundance during the EoR is still poorly constrained due to limited observations. Here, we use a physics-driven model to forecast future radio-loud quasar observations. We fit the parameters of the model using observational data of high-redshift quasars. Assuming Eddington accretion, the model yields an average lifetime of  $t_q \sim 10^{5.3}$  yr for quasars at  $z \sim 6$ , consistent with recent results obtained from quasar proximity zone pre-study. We show that if the radio-loud fraction of quasars evolves with redshift, it will significantly reduce the abundance of observable radio-loud quasars in the SKA era, making 21-cm forest studies challenging. With a constant radio-loud fraction, our model suggests that a one-year sky survey conducted with SKA-LOW has the capability to detect approximately 20 radio-loud quasars at  $z \sim 9$ , with sufficient sensitivity to resolve individual 21-cm forest lines.

**Keywords:** Quasars (1319) — Radio loud quasars (1349) — Reionization (1383) — H I line emission (690)

## 1. INTRODUCTION

The origin and evolution of stars, galaxies, and supermassive black holes in the universe are among the great unsolved mysteries of cosmology. Unveiling these enigmas requires probing the first billion years of cosmic history. The exploration of the cosmic dawn and the epoch of reionization (EoR) primarily rely on the use of the 21-cm hyperfine structure spectral line of neutral hydrogen atoms. Detecting the 21-cm cosmological signal is extremely challenging, but once a breakthrough is achieved, its scientific significance is enormous (Furlanetto et al. 2006; Morales & Wyithe 2010; Pritchard & Loeb 2012; Xu & Zhang 2020).

Probing the 21-cm signals of hydrogen atoms in the early universe mainly relies on the cosmic microwave background as the background radio source, detecting the absorption signals from the dark ages and the cosmic dawn, or the emission signals during the EoR when the gas is heated up by the early galaxies. Due to cosmic expansion, these 21-cm signals have been redshifted to low-frequency radio band, typically requiring low-frequency radio telescopes for observation. Currently, experiments to detect the cosmic dawn and EoR are in full swing, including experiments to detect the sky-averaged spectrum of the 21-cm signal during the cosmic dawn, such as Experiment to Detect the Global EoR Signature (EDGES) (Bowman et al. 2018), Shaped Antenna measurement of the background RAdio Spectrum (SARAS) (Singh et al. 2018), Hongmeng Project (Chen et al. 2023), Mapper of the IGM Spin Temperature (MIST) (Monsalve et al. 2024), The Radio Experiment for the Analysis of Cosmic Hydrogen (REACH) (de Lera Acedo et al. 2022), Probing Radio Intensity at high-Z from Marion (PRIZM) (Philip et al. 2019), The Large-

Corresponding author: Xin Zhang  
zhangxin@mail.neu.edu.cn

Corresponding author: Yidong Xu  
xuyd@nao.cas.cn

aperture Experiment to Detect the Dark Age (LEDA) (Price et al. 2018), Probing Reionization of the Universe using Signal from Hydrogen (PRATUTH) (Sathyanarayana Rao et al. 2023), Dark Ages Polarimeter Pathfinder (DAPPR)<sup>1</sup> and the High-Z All-Sky Spectrum Experiment (HIGH-Z) (Navros 2022). Additionally, there are experiments to detect the 21-cm power spectrum during the EoR, such as Low Frequency Array (LOFAR) (Patil et al. 2017), Murchison Widefield Array (MWA) (Tingay et al. 2013), Precision Array for Probing the Epoch of Reionization (PAPER) (Parsons et al. 2010), Hydrogen Epoch of Reionization Array (HERA) (DeBoer et al. 2017), The upgraded Global Multi-Resolution Topography (uGMRT) (Gupta et al. 2017) and the New Extension Upgrading LOFAR (NenuFAR) (Munshi et al. 2024). In particular, the Square Kilometre Array (SKA) (Huynh & Lazio 2013) under construction will be the largest radio telescope to date. It has a large field of view, a broad band, and an ultra-high sensitivity, capable of taking tomographic images of ionizing intergalactic medium (IGM) (Koopmans et al. 2015), which will reveal more detailed information of the EoR and make an important contribution to understanding the origin of cosmic structures.

In addition to these three measurement modes, another method of observing 21-cm signals is known as the 21-cm forest. If there are radio-bright point sources at the EoR, such as radio-loud quasars and radio afterglows of high- $z$  gamma-ray bursts, neutral clumps along the line of sight would create individual absorption lines on the source spectra, forming forest-like features called the 21-cm forest (in analogy to the Lyman- $\alpha$  forest) (Carilli et al. 2002; Furlanetto & Loeb 2002; Furlanetto 2006; Xu et al. 2009, 2010). The observation of 21-cm forest is of great value for studying the properties of the IGM, as it is highly sensitive to the heating process caused by the formation of early galaxies (Xu et al. 2009, 2011; Ciardi et al. 2013), and also for constraining the abundance of small-scale structures, so as to measure the properties of dark matter (DM) (Shimabukuro et al. 2014, 2020; Kadota et al. 2021). Recently, it was found that the one-dimensional cross power spectrum measurement of the 21-cm forest can be used to help extract faint 21-cm signals, and can also further measure the properties of DM and the early galaxies simultaneously (Shao et al. 2023).

The utilization of the 21-cm forest method is presently limited by three factors. Firstly, attaining the sensitivity necessary for detecting the 21-cm forest poses a challenge. Current radio telescopes such as LOFAR and MWA, lack the capability of conducting extensive detection deep into the EoR (Ciardi et al. 2013; Chatterjee et al. 2024). The anticipated completion of SKA in the near future will significantly mitigate

this existing detection challenge (Ciardi et al. 2015; Koopmans et al. 2015; Šoltinský et al. 2021). The vast effective aperture of SKA-LOW will empower us to detect the reionization process with unparalleled sensitivity. Secondly, there is a lack of an analytical model to connect physical parameters (such as dark matter mass and IGM temperature, etc.) with the 21 cm forest observational signals, making it difficult to carry out observational constraints on physical parameters (note that parameter inference based on large-scale simulations is extremely resource-intensive). To address this issue, we can consider constructing an analytical model. Alternatively, it is also possible to utilize methods based on deep learning. Recently, Sun et al. (2024) have developed a set of deep learning-based data generation and likelihood-free parameter inference methods to simultaneously address the issues of the absence of an analytical model and small-scale non-Gaussianity. Thirdly, the 21-cm forest necessitates high-redshift radio point sources as backgrounds. Owing to observational limitations, our understanding of the abundance of high-redshift radio sources remains limited, constituting the foremost uncertainty in the application of the 21-cm forest.

Quasars are one of the brightest sources in the universe, with about 10% of quasars exhibiting strong radio emissions (Stern et al. 2000; Ivezić et al. 2002; Bañados et al. 2015; Gloudemans et al. 2021; Liu et al. 2021). These radio-loud quasars serve as ideal background sources for 21-cm forest. With the continuous advancement of optical and near-infrared detection, the frontier of observing quasar redshift has reached 7.64 (Wang et al. 2021). However, there are only 8 quasars observed with redshift exceeding 7 and 14 radio-loud quasars observed with redshift exceeding 6 (McGreer et al. 2006; Willott et al. 2010; Bañados et al. 2015, 2021; Ighina et al. 2021; Liu et al. 2021; Gloudemans et al. 2022; Bañados et al. 2023; Ighina et al. 2023). During the deeper reionization epochs at higher redshifts, it is crucial to obtain theoretical estimates to determine whether there are sufficient radio-loud quasars available for 21-cm forest research.

To predict the abundance of high-redshift radio quasars, Haiman et al. (2004) (hereafter H04) developed a model driven by physical processes. By assuming a correspondence between supermassive black holes (SMBHs) and halos, as well as employing the Eddington limit for accretion, this model successfully derived the abundance of radio quasars consistent with observational data. After nearly two decades of equipment upgrades and observational data accumulation, we have gained further understanding of some of the physical and statistical properties of high-redshift quasars (e.g. Shang et al. 2011; Runnoe et al. 2012; Matsuoka et al. 2018; Shimasaku & Izumi 2019; Yang et al. 2021; Matsuoka et al. 2023; Šoltinský et al. 2023; Keller et al. 2024). Currently, some assumptions of the H04 model are challenged by observational data, requiring reasonable extensions and calibra-

<sup>1</sup> <https://www.colorado.edu/project/dark-ages-polarimeter-pathfinder/>

tions to fit the actual distribution of high-redshift quasars. This paper aims to update this model and make reasonable predictions for radio-loud quasar observations in the SKA era.

This paper is structured as follows. In Section 2, we describe the construction of the model and its calibration using high-redshift observational data. In Section 3, we present predictions for future SKA-LOW observations of radio-loud quasars and discuss the impact of currently poorly constrained parameters on the results. In Section 4, we give a summary of our findings and their implications. For this study, we have presumed the  $\Lambda$ CDM model and have used the cosmological parameters as measured by *Planck 2018* (Planck Collaboration et al. 2020):  $\Omega_m = 0.3111$ ,  $\Omega_\Lambda = 0.6889$ ,  $\Omega_b = 0.03314$ ,  $h = 0.6766$ ,  $\sigma_8 = 0.8102$ , and  $n_s = 0.9665$ .

## 2. METHOD

In this section, we focus on demonstrating the construction process of the model and discussing the rationality of some physical assumptions, eventually providing a calibrated model suitable for observing high-redshift ( $z \sim 6$ ) quasars. The calibration of the model uses quasar UV luminosity functions data at  $z \sim 6$  (Matsuoka et al. 2018) and  $z \sim 6.8$  (Matsuoka et al. 2023), as well as the black hole masses and the DM halo masses they inhabit obtained from 49 quasars at  $z \sim 6$  (Shimasaku & Izumi 2019).

### 2.1. Halo Mass Function

Quasars are powered by SMBHs. Therefore, we first need to estimate the abundance of SMBHs at the centers of galaxies. We assume that the SMBH population traces DM halos, and the distribution of DM halos follows the Sheth-Tormen form (Sheth & Tormen 2002),

$$f(\sigma, z) = 0.322 \sqrt{\frac{3}{2\pi}} \frac{\delta_c}{\sigma} \left( 1 + \left( \frac{4\sigma^2}{3\delta_c^2} \right)^{0.3} \right) \exp \left[ -\frac{3\delta_c^2}{8\sigma^2} \right], \quad (1)$$

where  $\delta_c = 1.6865$  is the threshold density for spherical collapse.  $\sigma$  is the density fluctuation,

$$\sigma^2(M, z) = \sigma^2(R_{\text{sph}}, z) = \int_0^\infty \frac{dk}{2\pi^2} k^2 P(k, z) \left[ \frac{3j_1(kR_{\text{sph}})}{kR_{\text{sph}}} \right]^2, \quad (2)$$

where  $j_1(x) = (\sin x - x \cos x)/x^2$ ,  $R_{\text{sph}}$  is the comoving radius related to mass  $M$  by  $M = 4\pi\rho_m R_{\text{sph}}^3/3$ . The cosmological power spectrum  $P(k, z)$  is calculated using the fitting form of Eisenstein & Hu (1999). Since we are discussing quasars during the cosmic reionization when DM halos had not undergone large-scale mergers, this assumption is reasonable.

### 2.2. Halo-SMBH Mass Relation

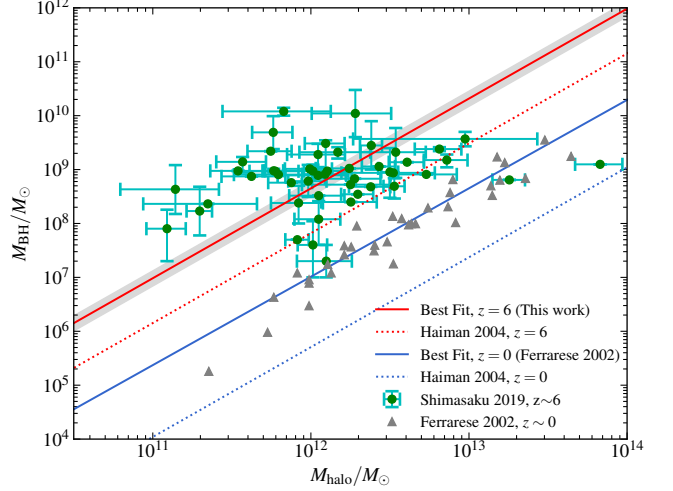


**Figure 1.**  $M_{\text{halo}} - M_{\text{BH}}$  relation. The red lines represent  $z = 6$ , and the blue lines represent  $z = 0$ . Solid lines represent observational fitting, while dashed lines represent the mass relation used by H04. The shaded area represents the  $1\sigma$  error. The gray triangular data points are from Ferrarese (2002), and the green data points are from Shimasaku & Izumi (2019).

By assuming that the radiation feedback and outflows of quasars determine the size of black holes, we can obtain the scaling relationship between black hole mass and DM halo mass (Silk & Rees 1998; Haehnelt et al. 1998; Wyithe & Loeb 2003). The mass scaling relationship is expressed as (Equation (4) in Wyithe & Loeb (2003)):

$$M_{\text{BH}} = A \left( \frac{M_{\text{halo}}}{1.5 \times 10^{12} M_\odot} \right)^{5/3} \left[ \frac{\xi(z)}{\Omega_m} \right]^{5/6} (1+z)^{5/2} M_\odot, \quad (3)$$

where  $M_{\text{BH}}$  is the black hole mass,  $M_{\text{halo}}$  is the DM halo mass,  $A$  is the amplitude parameter,  $\xi(z)$  is the dimensionless parameter related to redshift  $z$ , and  $\xi(z) \simeq \Omega_m$  for  $z \geq 6$ .

We note that H04 used quasar luminosity function data at  $z \gtrsim 3$  to fit the amplitude parameter, with the average quasar lifetime fixed at  $2 \times 10^7$  years. However, the results obtained did not match the observations of the local universe and those at redshift 6 (see Figure 1). Note that recent studies on quasar lifetimes suggest shorter lifetimes (Eilers et al. 2017, 2021; Morey et al. 2021), and in our analysis, the average quasar lifetime is treated as a variable and is constrained by high-redshift luminosity function data (see Section 2.4). To better predict the distribution of high-redshift quasars, we used the SMBH and halo masses obtained from observational data of 49 quasars at  $z \sim 6$  (Shimasaku & Izumi 2019) to fit the amplitude parameter (red solid line in Figure 1). We found that the best fit amplitude parameter  $A = 10^{6.83}$  is approximately 7 times the amplitude used by H04.

### 2.3. Accretion Rate and Optical Luminosity

We assume that the average Eddington ratio  $\lambda_{\text{Edd}}$  for high-redshift quasars is 1, indicating Eddington accretion. Al-

though the average accretion rate of quasars in the local universe is much lower than Eddington accretion, recent high-redshift observations suggest that the average Eddington ratio of early quasars is close to 1 (Yang et al. 2021). Additionally, we note that to explain the formation of SMBHs represented by the observed high-redshift quasars, some studies have adopted models of sustained mild super-Eddington accretion (e.g. Pacucci et al. 2015; Li et al. 2023) or chaotic accretion (e.g. Zubovas & King 2021). The results of Lupi et al. (2023) indicate that super-Eddington accretion can also persist for a long time. Based on the above observation and simulation results, we believe our assumption is reasonable.

Once we determine the Eddington ratio, we can calculate the optical luminosity of quasars. Assuming a quasar has an average Eddington ratio of  $\lambda_{\text{Edd}}$  over its lifetime, we can get the bolometric luminosity as

$$L_{\text{bol}} = \lambda_{\text{Edd}} L_{\text{Edd}}, \quad (4)$$

where  $L_{\text{Edd}}$  is the Eddington luminosity. As the discussion above, we adopt  $\lambda_{\text{Edd}} = 1$  for most of our calculations. As an additional discussion, we also calculated the case of  $\lambda_{\text{Edd}} = 1.2$ .

For quasar bolometric luminosity corrections, we use the results of Runnoe et al. (2012) (their Equations (11) and (13)),

$$\log(L_{\text{bol}}) = \log(0.75) + 4.89 + 0.91 \times \log(5100 L_{5100}). \quad (5)$$

We use the average spectral energy distribution from Shang et al. (2011) to calculate the luminosity relationship between different optical bands.

#### 2.4. Duty Cycle of Quasar Phase

Through the halo mass function and the halo-SMBH mass relation, we have obtained the abundance of black holes. However, not all black holes are in the quasar phase at the same time. We need to estimate the proportion of black holes that are in the quasar phase, which is the duty cycle. We estimate the duty cycle as

$$D_q = \frac{t_q}{t_H(z)}, \quad (6)$$

where  $t_q$  is the average lifetime of quasars, and  $t_H(z)$  is the age of the universe at redshift  $z$ .

The average lifetime  $t_q$  and average accretion rate  $\lambda_{\text{Edd}}$  of quasars are strongly correlated parameters. We obtained the best fit to the observed luminosity function data by varying the average lifetime  $t_q$  of the quasars, using a fixed average Eddington ratio  $\lambda_{\text{Edd}} = 1$  for early quasars. We employed two sets of high-redshift observational data, obtained from observations of  $z \sim 6$  (Matsuoka et al. 2018) and  $z \sim 6.8$  (Matsuoka et al. 2023). Our best-fit results are shown in Figure 2,

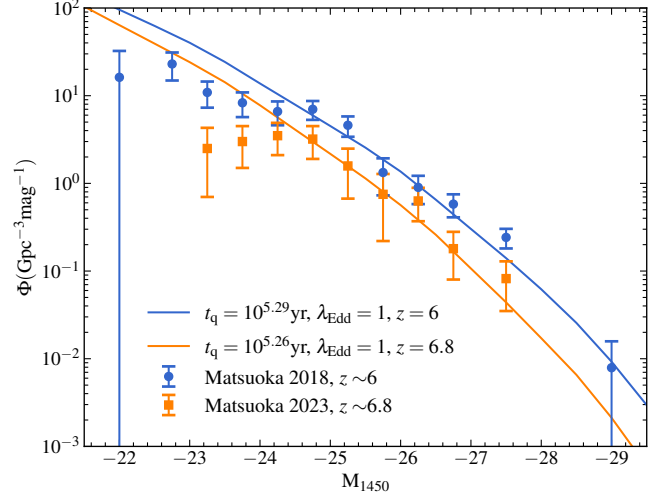


**Figure 2.** UV luminosity function fitting results. The average Eddington ratio of quasars is fixed at 1. The blue line represents  $z = 6$ , and the orange line represents  $z = 6.8$ . Solid lines represent model best fits. Note that we ignored the first two points on the faint end during fitting due to observational incompleteness. The data points are provided by Matsuoka et al. (2018) and Matsuoka et al. (2023).

and we take the logarithmic mean value  $10^{5.275}$  yr in subsequent calculations. Note that both sets of data, especially the  $z \sim 6.8$  data, are affected by incomplete observation coverage at the faint end, so we did not use the first two data points at the faint end in the fitting process. As a possible scenario, we also calculated the fit with an average Eddington ratio of  $\lambda_{\text{Edd}} = 1.2$ , which is shown in Figure 3.

We note that Bolgar et al. (2018) used a constant duty cycle of  $D_q = 0.02$  to fit the observed optical luminosity function. However, Haimes & Loeb (1998) and Haehnelt et al. (1998) pointed out a connection between the duty cycle and Equation (3). If the amplitude factor  $A$  in Equation (3) is changed, the resulting duty cycle will also change. Since the amplitude factor  $A$  we use is different from that of Bolgar et al. (2018), the resulting duty cycle is also different. Note that our amplitude factor  $A$  and duty cycle  $D_q$  are fitted from observational data at  $z \sim 6$ , so the resulting duty cycle is only applicable to high redshifts.

#### 2.5. Radio-Loud Fraction

We assume that the radio-loud fraction (RLF) of quasars at high redshift is 10%. This assumption is consistent with observational studies of the RLF up to redshift of  $z \sim 6$  (Stern et al. 2000; Ivezić et al. 2002; Bañados et al. 2015; Gloude-mans et al. 2021; Liu et al. 2021). We also note that Jiang et al. (2007) proposed a form for the evolution of the RLF with redshift and luminosity,

$$\log\left(\frac{\text{RLF}}{1 - \text{RLF}}\right) = b_0 + b_z \log(1 + z) + b_M (M_{2500} + 26), \quad (7)$$



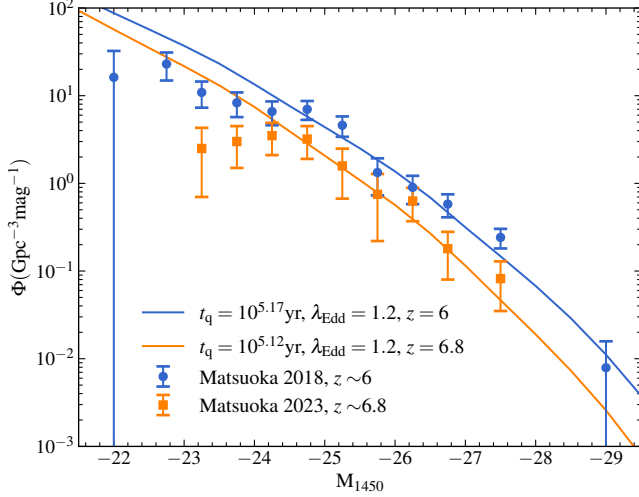


**Figure 3.** Similar to Figure 2. The average Eddington ratio of quasars is fixed at 1.2.

where  $M_{2500}$  represents the optical magnitude at 2500Å.  $b_0$ ,  $b_z$  and  $b_M$  are free parameters, with best-fit values of  $-0.132$ ,  $-2.052$ , and  $-0.183$ , respectively. Since the recent study on the RLF of  $z \geq 6$  quasars does not rule out the possibility of this form of evolution (Keller et al. 2024), we also calculated its impact on the results (see Section 3.5).

### 2.6. Radio-Loudness Distribution

We used the radio loudness data of 225 radio-loud quasars with redshift from 0 to 5 from Bariuan et al. (2022) to perform a Gaussian fit of the radio-loudness distribution. The definition of radio-loudness is the logarithm of the ratio of the rest frame luminosity between 5 GHz and 4400Å ( $R = \log_{10}(L_{5\text{GHz}}/L_{4400})$ ). We estimate the radio-loudness distribution of the radio loud quasars to be

$$N(R) = \frac{1}{\sqrt{2\pi}\sigma_0} \exp\left(-\frac{(R-\bar{R})^2}{2\sigma_0^2}\right), \quad (8)$$

where  $R$  is radio-loudness, and  $\bar{R}$  and  $\sigma_0$  are free parameters. Figure 4 shows the result of our radio-loudness distribution fitting, with the best fitting result being  $\bar{R} = 2.67$  and  $\sigma_0 = 0.55$ . We also performed fits for the high-redshift and low-redshift data separately and did not find any significant evidence of redshift evolution. Therefore, we believe that applying this distribution form to higher redshifts should be safe.

### 2.7. Radio Spectral Index

To calculate the radio luminosity of a particular band, we assume that the radio spectrum conforms to the following relation,

$$F_{\text{radio}} \propto \nu^\alpha, \quad (9)$$

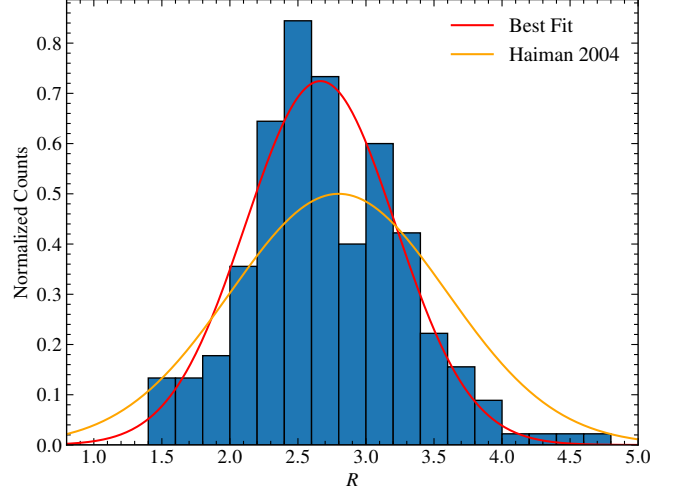


**Figure 4.** The fitting results of the radio-loudness distribution. The radio-loudness data used are from Bariuan et al. (2022). The red line represents our best fit to the data, the orange line represents the radio-loudness distribution H04 used.

where  $F_{\text{radio}}$  is the radio flux and  $\alpha$  is the radio spectral index. The radio spectral index affects two calculation processes: one involves converting from the observational frame to the rest frame, known as K-correction, and the other is the transformation between the 5 GHz definition of radio-loudness and the SKA-LOW observing band. Based on the findings of Gloudemans et al. (2021), who derived a median spectral index of  $-0.29$  through the stacking of 93 quasars using Low Frequency Array Two Metre Sky survey (LoTSS-DR2) and Faint Images of the Radio Sky at Twenty Centimeters (FIRST) data, we adopt  $\alpha = -0.29$ . Note that previous high-redshift studies based on a small number of observational data used a steeper spectral index of  $\alpha = -0.75$ . Our spectral index value is supported by a larger sample ( $93 z > 5$  quasars), which should be more reliable. Due to our limited understanding of high-redshift quasar radio spectra, we also calculated the impact of  $\alpha = -0.75$  on the results as a possible scenario (see Section 3.4).

### 2.8. Radio-Loud Quasar Abundance

From the above definition, we can get the radio-loud quasar abundance with flux greater than a certain flux threshold  $F_{\text{radio}}$  as

$$\frac{dN}{dzd\Omega}(F_{\text{radio}}, z) = \frac{dV}{dzd\Omega} D_q \times \int_0^\infty dM_{\text{halo}} \left( \int_{R_0(M_{\text{halo}}, F_{\text{radio}})}^\infty dR N(R) \right) \frac{dn}{dM_{\text{halo}}}, \quad (10)$$

where  $dV/dzd\Omega$  is the cosmological volume element,  $R_0$  is the threshold of radio loudness calculated from the given radio flux density threshold  $F_{\text{radio}}$  and halo mass  $M_{\text{halo}}$ , and  $dn/dM_{\text{halo}}$  is the halo abundance calculated from Equation (1).

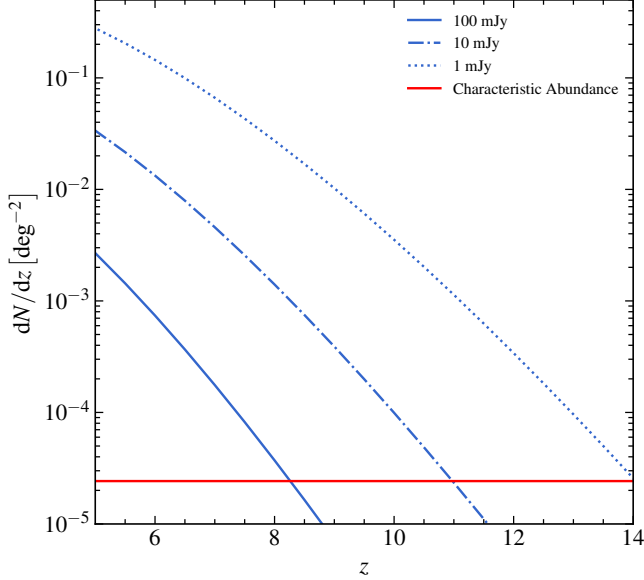


**Figure 5.** Predicted distribution of radio-loud quasar abundance above different flux thresholds as a function of redshift, with the observation band at 150 MHz. The characteristic abundance  $\Phi^*$  corresponds to an abundance where the expected number of observations over the entire sky ( $\sim 41253 \text{ deg}^2$ ) is 1 ( $\Phi^* \simeq 1/41253 \text{ deg}^{-2}$ ). Sources with an abundance below this value are almost non-existent.

### 3. RESULTS AND DISCUSSIONS

#### 3.1. Quasar Abundance Predicted by The Model

Figure 5 shows the distribution of quasar abundance above a given radio flux threshold as a function of redshift, obtained according to Equation (10). As discussed in Section 2, the standard parameter settings we used are as follow: average Eddington ratio  $\lambda_{\text{Edd}} = 1$ , average quasar lifetime  $t_q = 10^{5.275}$  years, radio spectral index  $\alpha = -0.29$ , and radio-loudness fraction RLF = 10%.

#### 3.2. Comparison with LOFAR Observations

We attempt to compare the calibrated model with existing high-redshift radio observations. Specifically, we use data from the EALIS-N1 field in the LoSST Deep Fields DR1 (Sabater et al. 2021; Best et al. 2023), which has the lowest average noise level in the three deep fields. We select radio-excess AGNs with redshifts between 5.6 and 6.4 from this deep field observation data and construct the radio luminosity function using the standard  $1/V_{\text{max}}$  technique (Schmidt 1968; Condon 1989). The detailed calculation process and incompleteness information can be found in Section 3.1 of Kondapally et al. (2022). For the model, we convolve the optical luminosity function with the radio-loudness distribution to calculate the radio luminosity function. Figure 6 shows the comparison of the radio luminosity function predicted by the model with the LOFAR observations. At  $z \sim 6$ , the model-predicted radio luminosity function matches well

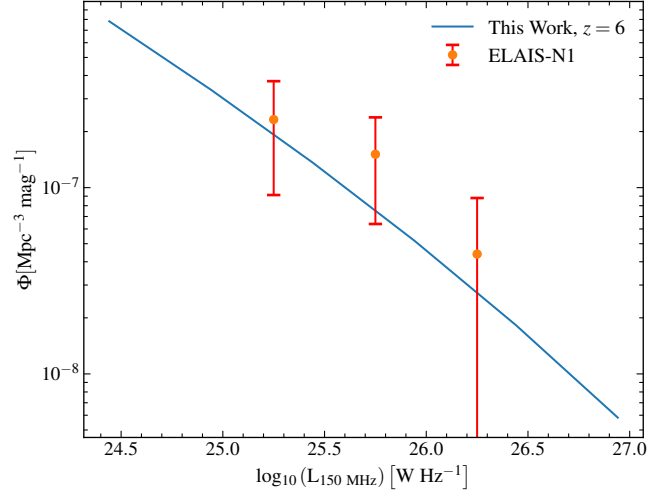


**Figure 6.** Comparison of the radio luminosity function with observational data. The blue line represents the radio luminosity function of radio-loud quasars at  $z = 6$  calculated by the model, while the red data points are the observational results from the EALIS-N1 field in the LoSST Deep Fields DR1, with error bars representing the  $1\sigma$  error.

with the LOFAR observations. However, we also notice that the observed radio luminosity function is slightly higher than the model prediction (within the error range), and this discrepancy is more pronounced in the Lockman Hole field (exceeding the  $1\sigma$  error range). Since our model is calibrated using the observed optical luminosity function, this discrepancy may indicate that some high accretion rate AGNs during the reionization epoch are optically obscured, which is consistent with some recent high-redshift researches (Endsley et al. 2023; Lambrides et al. 2024; Banados et al. 2024).

#### 3.3. SKA-LOW Observation Forecast

For SKA-LOW radio-loud quasar observations, we considered two observation modes: the first is a survey to search for quasars. Since the goal of this survey is to find visible radio-loud quasars in the sky, a high frequency resolution is not required, so we refer to it as a continuum survey. The relevant parameters for the continuum survey are summarized in Table 1. The second mode is a survey to find radio-loud quasars suitable for 21-cm forest studies. To resolve individual 21-cm lines, this survey requires higher frequency resolution, and thus we call it the 21-cm forest survey. The relevant parameters for the 21-cm forest survey are summarized in Table 2. Note that our 21-cm forest survey forecast shows the total number of sources within a survey area of  $10313 \text{ deg}^2$  that can resolve individual 21-cm lines with 100 h of integration time. Conducting a 21-cm forest blind survey with this setup would require a substantial amount of observation time ( $\sim 9$  years). From an observational perspective, we should first conduct the continuum blind survey to determine the positions of visible sources and then perform a high

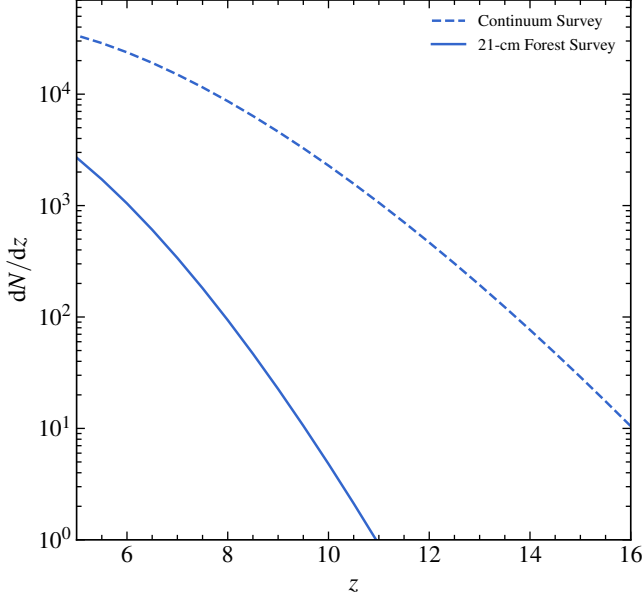


**Figure 7.** Forecast of the SKA-LOW observations. Dash lines represent continuum survey, and solid lines represent 21-cm forest survey. The parameters for continuum survey and 21-cm forest survey are shown in Table 1 and Table 2, respectively.

frequency-resolution follow-up observations on those bright sources. How to filter high-redshift candidates from the blind survey results is an important issue for future observations, which is not discussed in this paper.

To predict the observations of SKA-LOW, we estimate the noise using the following formula (Thompson et al. 2017),

$$\delta S^N \approx \frac{2k_B T_{\text{sys}}}{A_{\text{eff}} \sqrt{2\delta\nu\delta t}}, \quad (11)$$

where  $A_{\text{eff}}$  is the effective collecting area of the telescope,  $T_{\text{sys}}$  is the system temperature,  $\delta\nu$  is the channel width and  $\delta t$  is the integration time. For continuum survey, the single-field integration time  $\delta t$  is determined by the survey coverage  $S_{\text{tot}}$  and the total survey time  $T_{\text{tot}}$ ,

$$\delta t = \frac{T_{\text{tot}}}{S_{\text{tot}}/\Omega}, \quad (12)$$

where  $\Omega$  is the field of view, given by  $\Omega \approx (1.2\lambda/D_{\text{ant}})^2$ . We estimate  $\Omega$  using the wavelength corresponding to 150 MHz. We assume that the signal-to-noise ratio is greater than 5 to detect quasars. For continuum survey, this means  $\text{Flux} > 5 \times \delta S^N$ . For 21-cm forest survey, we assume an optical depth of  $\tau = 0.1$  on the basis of a signal-to-noise ratio of 5, which means  $\text{Flux} \times (1 - e^{-\tau}) > 5 \times \delta S^N$ .

Figure 7 shows the model's predictions for one year of SKA-LOW observations. At redshifts above 9, we expect to observe a large number of radio-loud quasars, among which approximately 20 quasars are bright enough to resolve individual 21-cm lines. This number of radio-loud quasar is

**Table 1.** Proposed observation parameters for SKA-LOW Continuum Survey.

Parameter	Symbol	Value	Unit
Search Coverage	$S_{\text{tot}}$	10313	$\text{deg}^2$
Survey Time	$T_{\text{tot}}$	$365 \times 6$	hours
Effective Collecting Area	$A_{\text{eff}}$	419000	$\text{m}^2$
Channel Width	$\delta\nu$	10	MHz
Antenna Diameter	$D_{\text{ant}}$	40	m
System Temperature	$T_{\text{sys}}$	$40 + 1.1T_{\text{gal}}$	K

**Note.** Instrument parameters are obtained from [Square Kilometre Array Cosmology Science Working Group et al. \(2020\)](#). The observation time is assumed to be one year, and the effective observation time is 6 hours per day.  $T_{\text{gal}} = 25 \left( \frac{408 \text{ MHz}}{f(z)} \right)^{2.75}$ , where  $f(z)$  is the frequency at redshift  $z$ .

**Table 2.** Proposed observation parameters for SKA-LOW 21-cm forest survey.

Parameter	Symbol	Value	Unit
Sky Coverage	$S_{\text{tot}}$	10313	$\text{deg}^2$
Integration Time	$\delta t$	100	hours
Effective Collecting Area	$A_{\text{eff}}$	419000	$\text{m}^2$
Channel Width	$\delta\nu$	5	kHz
Antenna Diameter	$D_{\text{ant}}$	40	m
System Temperature	$T_{\text{sys}}$	$40 + 1.1T_{\text{gal}}$	K

**Note.** Similar to Table 1, the integration time and the channel width vary. See Section 3.3 for the observation strategy.

enough to make the 21-cm forest an effective probe for the EoR. Note that we assume an effective daily observation time of 6 hours for the survey, which is a conservative estimate. Therefore, the actual number of quasars that can serve as 21-cm forest background sources is expected to be higher than our predictions.

### 3.4. Influence of Radio Spectral Index

Figures 8 and 9 show the influence of different radio spectral indices on the results. Typically, we use  $-0.5$  as a standard to determine whether a radio spectrum is steep or flat. Early radio studies of galaxies suggested a steep radio spectral index of  $-0.75$  (Condon 1992), which has been adopted by multiple studies (e.g., Wang et al. 2007; Momjian et al. 2014; Bañados et al. 2015). We note that recently Gloude-mans et al. (2021) used observational data from 93 quasars with  $z > 5$  to constrain the radio spectral index, obtaining a result of  $-0.29$ . Since our understanding of the radio spectra of quasars is still limited, here we calculate the influence of multiple values of radio spectral indices on the results.

### 3.5. Influence of Radio Loud Fraction

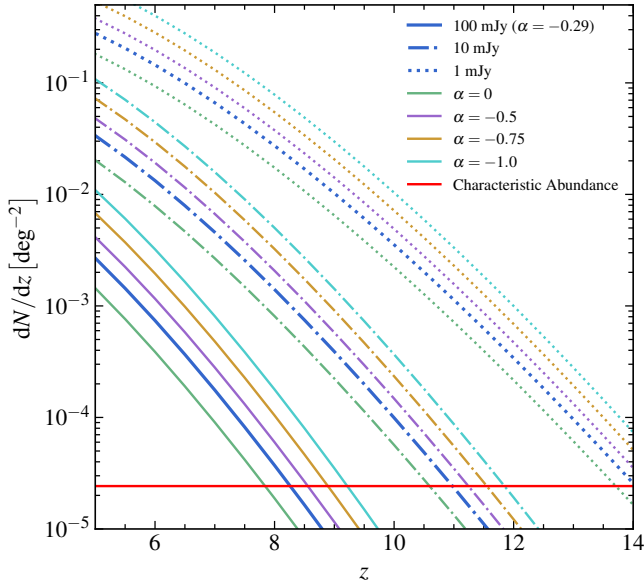


**Figure 8.** Influence of different radio spectral index settings on the abundance of radio-loud quasars. Different colors of lines represent different spectral indices, while different line styles represent different radio flux thresholds (150 MHz flux). Sources with an abundance below the characteristic abundance marked by the red line are almost non-existent.

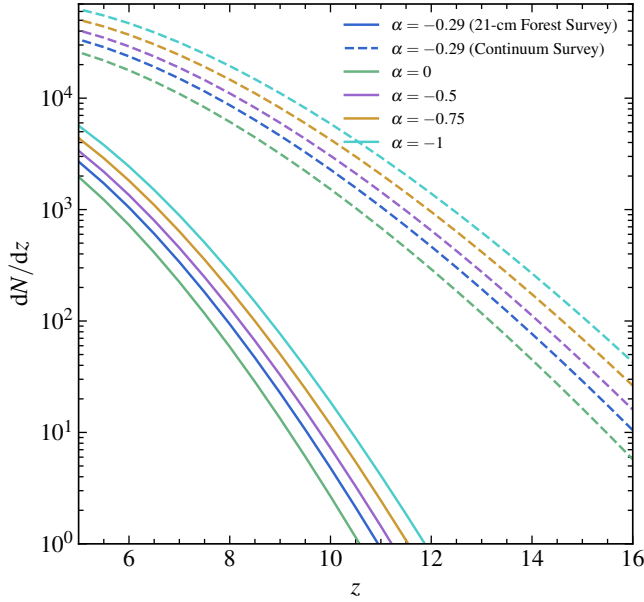


**Figure 9.** Influence of different radio spectral index settings on the forecast results of SKA-LOW observations. The observation frequency band of SKA-LOW is used for calculations here. Specifically, for continuum surveys, we used 150 MHz, while for 21-cm forest survey, we used the frequency of the redshifted 21-cm line.

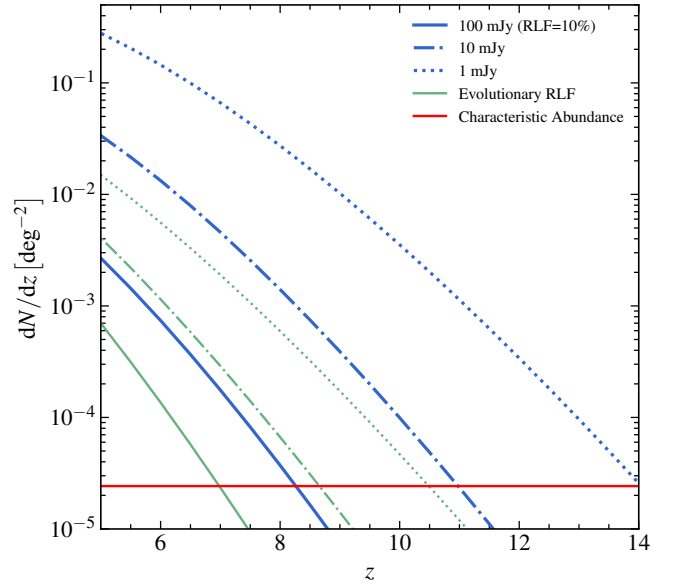


**Figure 10.** Influence of evolving RLF on the abundance of radio-loud quasars. The blue line represents a constant 10% RLF, while the green line represents an evolving RLF. Different line styles indicate different radio flux thresholds (150 MHz flux). Sources with an abundance below the characteristic abundance marked by the red line are almost non-existent.

Figures 10 and 11 illustrate the impact of the evolution of RLF with redshift and luminosity on the results. We adopted the evolutionary form from Jiang et al. (2007), which implies that the RLF at high redshift is much lower than 10%. Under the assumption of evolutionary RLF, the model predicts a significant decrease in the abundance of quasars observable by SKA-LOW's one-year survey, making it more challenging to use the 21-cm forest method to probe cosmic reionization. If this RLF evolution is real, during the reionization period, the number of quasars with 100-hour integration times sufficient to resolve individual 21-cm lines is insufficient to support the 21-cm forest method, and we may need longer observation times to utilize relatively fainter quasars.

#### 4. CONCLUSION

One of the interesting results obtained from our model is the average lifetime  $t_q$  of high-redshift ( $z \gtrsim 6$ ) quasars. Assuming Eddington accretion, the observed high-redshift quasar luminosity function requires that the average lifetime of quasars given by the model is  $\sim 10^5$  years (see Section 2.4). Although this result is much smaller than early theoretical estimates ( $\sim 10^7$  years), it is close to recent constraints using Ly $\alpha$  near-zone data. Note that determining the average lifetime of quasars in the model requires a given halo-SMBH mass relationship, and currently there is large uncertainty in the estimation of high-redshift SMBH and halo masses based on quasar spectra. It is foreseeable that with the accumulation of high-redshift observational data, our model can pro-



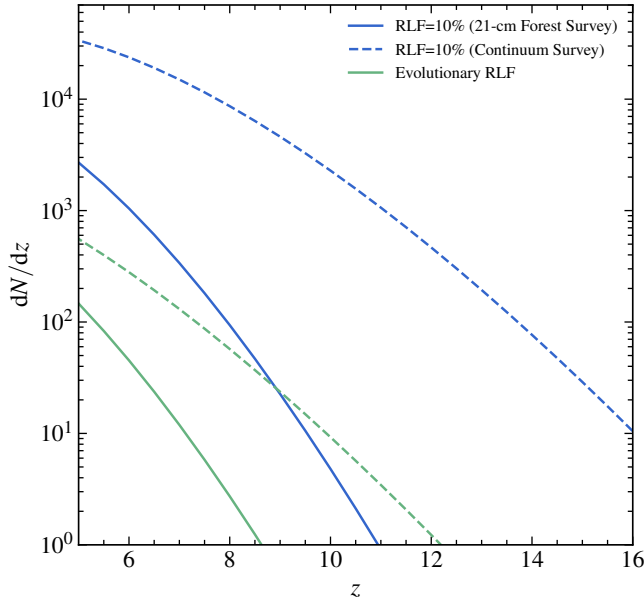


**Figure 11.** Influence of evolving RLF on the forecast results of SKA-LOW observations. The blue line represents a constant 10% RLF, while the green line represents an evolving RLF. The dash line represents the continuum survey, and the solid line represents the 21-cm forest survey. Detailed descriptions of the continuum survey and the 21-cm forest survey can be found in Section 3.3.

vide a more reliable average lifetime of quasars, which will help us understand the growth process of SMBHs in the early universe.

Another notable finding concerns the accretion behavior of AGNs. Our model, calibrated at high redshift, indicates that quasars have high accretion rates and short lifetimes. However, applying this setting to lower redshift results in significant discrepancies with observations. As a simple attempt, we recalibrated the model using the quasar luminosity function at  $z = 4$ , resulting in an average Eddington ratio of  $\lambda_{\text{Edd}} = 0.04$  and an average quasar lifetime of  $t_q = 10^{8.2}$  years. This suggests that the accretion behaviors of early and late AGNs differ greatly.

The most significant result derived from our model is the prediction of the abundance of radio-loud quasars observable by SKA-LOW in a one-year survey. According to the standard parameter settings (Figure 7), we expect to identify over a thousand radio-loud quasars at  $z > 6$  that are sufficient to

resolve individual 21-cm lines, within a year of observation. Even at higher redshifts, such as  $z > 9$ , we can still detect approximately 20 such radio-loud quasars.

We tested the impact of various quasar radio spectral indices on our results (Figure 9). Our findings indicate that a steeper radio spectrum is more favorable for observations in the SKA-LOW frequency band. However, the radio spectral index has minimal effect on the results.

Our results suggest that the evolution of RLF is a looming issue for 21-cm forest in the SKA era (Figure 11). If the RLF remains close to 10% at high redshift, then the 21-cm forest can serve as an effective probe of reionization. However, if the RLF evolution claimed by Jiang et al. (2007) is real, detecting 21-cm forest background sources will be challenging, and we may need longer integration times to utilize relatively fainter quasars.

## ACKNOWLEDGMENTS

We thank K. Shimasaku for providing us with the compiled data of the halo–SMBH mass relation. This work was supported by the National SKA Program of China (Grants Nos. 2022SKA0110200, 2022SKA0110203, 2020SKA0110401, and 2020SKA0110100), the National Natural Science Foundation of China (Grants Nos. 11975072, 11875102, and 11835009), the National 111 Project (Grant No. B16009), the CAS Project for Young Scientists in Basic Research (Grant No. YSBR-092), the National Key R&D Program of China (Grant No. 2022YFF0504300), and the science research grants from the China Manned Space Project (Grants Nos. CMS-CSST-2021-B01 and CMS-CSST-2021-A02). LOFAR data products were provided by the LOFAR Surveys Key Science project (LSKSP; <https://lofar-surveys.org/>) and were derived from observations with the International LOFAR Telescope (ILT). LOFAR (van Haarlem et al. 2013) is the Low Frequency Array designed and constructed by ASTRON. It has observing, data processing, and data storage facilities in several countries, which are owned by various parties (each with their own funding sources), and which are collectively operated by the ILT foundation under a joint scientific policy. The efforts of the LSKSP have benefited from funding from the European Research Council, NOVA, NWO, CNRS-INSU, the SURF Co-operative, the UK Science and Technology Funding Council and the Jülich Supercomputing Centre.

## REFERENCES

- Bañados, E., Venemans, B. P., Morganson, E., et al. 2015, *ApJ*, 804, 118, doi: [10.1088/0004-637X/804/2/118](https://doi.org/10.1088/0004-637X/804/2/118)
- Bañados, E., Mazzucchelli, C., Momjian, E., et al. 2021, *ApJ*, 909, 80, doi: [10.3847/1538-4357/abe239](https://doi.org/10.3847/1538-4357/abe239)
- Bañados, E., Schindler, J.-T., Venemans, B. P., et al. 2023, *ApJS*, 265, 29, doi: [10.3847/1538-4365/acb3c7](https://doi.org/10.3847/1538-4365/acb3c7)
- Bañados, E., Momjian, E., Connor, T., et al. 2024, *arXiv e-prints*, arXiv:2407.07236, doi: [10.48550/arXiv.2407.07236](https://doi.org/10.48550/arXiv.2407.07236)

- Bariuan, L. G. C., Snios, B., Sobolewska, M., Siemiginowska, A., & Schwartz, D. A. 2022, *MNRAS*, 513, 4673, doi: [10.1093/mnras/stac1153](https://doi.org/10.1093/mnras/stac1153)
- Best, P. N., Kondapally, R., Williams, W. L., et al. 2023, *MNRAS*, 523, 1729, doi: [10.1093/mnras/stad1308](https://doi.org/10.1093/mnras/stad1308)
- Bolgar, F., Eames, E., Hottier, C., & Semelin, B. 2018, *MNRAS*, 478, 5564, doi: [10.1093/mnras/sty1293](https://doi.org/10.1093/mnras/sty1293)
- Bowman, J. D., Rogers, A. E. E., Monsalve, R. A., Mozdzen, T. J., & Mahesh, N. 2018, *Nature*, 555, 67, doi: [10.1038/nature25792](https://doi.org/10.1038/nature25792)
- Carilli, C. L., Gnedin, N. Y., & Owen, F. 2002, *ApJ*, 577, 22, doi: [10.1086/342179](https://doi.org/10.1086/342179)
- Chatterjee, S., Elahi, K. M. A., Bharadwaj, S., et al. 2024, arXiv e-prints, arXiv:2405.10080, doi: [10.48550/arXiv.2405.10080](https://doi.org/10.48550/arXiv.2405.10080)
- Chen, X., Yan, J., Xu, Y., et al. 2023, *ChJSS*, 43, 43, doi: [10.11728/cjss2023.01.220104001](https://doi.org/10.11728/cjss2023.01.220104001)
- Ciardi, B., Inoue, S., Mack, K., Xu, Y., & Bernardi, G. 2015, in *Advancing Astrophysics with the Square Kilometre Array (AASKA14)*, 6, doi: [10.22323/1.215.0006](https://doi.org/10.22323/1.215.0006)
- Ciardi, B., Labropoulos, P., Maselli, A., et al. 2013, *MNRAS*, 428, 1755, doi: [10.1093/mnras/sts156](https://doi.org/10.1093/mnras/sts156)
- Condon, J. J. 1989, *ApJ*, 338, 13, doi: [10.1086/167176](https://doi.org/10.1086/167176)
- . 1992, *ARA&A*, 30, 575, doi: [10.1146/annurev.aa.30.090192.003043](https://doi.org/10.1146/annurev.aa.30.090192.003043)
- de Lera Acedo, E., de Villiers, D. I. L., Razavi-Ghods, N., et al. 2022, *NatAs*, 6, 984, doi: [10.1038/s41550-022-01709-9](https://doi.org/10.1038/s41550-022-01709-9)
- DeBoer, D. R., Parsons, A. R., Aguirre, J. E., et al. 2017, *PASP*, 129, 045001, doi: [10.1088/1538-3873/129/974/045001](https://doi.org/10.1088/1538-3873/129/974/045001)
- Eilers, A.-C., Davies, F. B., Hennawi, J. F., et al. 2017, *ApJ*, 840, 24, doi: [10.3847/1538-4357/aa6c60](https://doi.org/10.3847/1538-4357/aa6c60)
- Eilers, A.-C., Hennawi, J. F., Davies, F. B., & Simcoe, R. A. 2021, *ApJ*, 917, 38, doi: [10.3847/1538-4357/ac0a76](https://doi.org/10.3847/1538-4357/ac0a76)
- Eisenstein, D. J., & Hu, W. 1999, *ApJ*, 511, 5, doi: [10.1086/306640](https://doi.org/10.1086/306640)
- Endsley, R., Stark, D. P., Lyu, J., et al. 2023, *MNRAS*, 520, 4609, doi: [10.1093/mnras/stad266](https://doi.org/10.1093/mnras/stad266)
- Ferrarese, L. 2002, *ApJ*, 578, 90, doi: [10.1086/342308](https://doi.org/10.1086/342308)
- Furlanetto, S. R. 2006, *MNRAS*, 370, 1867, doi: [10.1111/j.1365-2966.2006.10603.x](https://doi.org/10.1111/j.1365-2966.2006.10603.x)
- Furlanetto, S. R., & Loeb, A. 2002, *ApJ*, 579, 1, doi: [10.1086/342757](https://doi.org/10.1086/342757)
- Furlanetto, S. R., Oh, S. P., & Briggs, F. H. 2006, *PhR*, 433, 181, doi: [10.1016/j.physrep.2006.08.002](https://doi.org/10.1016/j.physrep.2006.08.002)
- Gludemans, A. J., Duncan, K. J., Röttgering, H. J. A., et al. 2021, *A&A*, 656, A137, doi: [10.1051/0004-6361/202141722](https://doi.org/10.1051/0004-6361/202141722)
- Gludemans, A. J., Duncan, K. J., Saxena, A., et al. 2022, *A&A*, 668, A27, doi: [10.1051/0004-6361/202244763](https://doi.org/10.1051/0004-6361/202244763)
- Gupta, Y., Ajithkumar, B., Kale, H. S., et al. 2017, *Csic*, 113, 707, doi: [10.18520/cs/v113/i04/707-714](https://doi.org/10.18520/cs/v113/i04/707-714)
- Haehnelt, M. G., Natarajan, P., & Rees, M. J. 1998, *MNRAS*, 300, 817, doi: [10.1046/j.1365-8711.1998.01951.x](https://doi.org/10.1046/j.1365-8711.1998.01951.x)
- Haiman, Z., & Loeb, A. 1998, *ApJ*, 503, 505, doi: [10.1086/306017](https://doi.org/10.1086/306017)
- Haiman, Z., Quataert, E., & Bower, G. C. 2004, *ApJ*, 612, 698, doi: [10.1086/422834](https://doi.org/10.1086/422834)
- Huynh, M., & Lazio, J. 2013, arXiv e-prints, arXiv:1311.4288, doi: [10.48550/arXiv.1311.4288](https://doi.org/10.48550/arXiv.1311.4288)
- Ighina, L., Belladitta, S., Caccianiga, A., et al. 2021, *A&A*, 647, L11, doi: [10.1051/0004-6361/202140362](https://doi.org/10.1051/0004-6361/202140362)
- Ighina, L., Caccianiga, A., Moretti, A., et al. 2023, *MNRAS*, 519, 2060, doi: [10.1093/mnras/stac3668](https://doi.org/10.1093/mnras/stac3668)
- Ivezić, Ž., Menou, K., Knapp, G. R., et al. 2002, *AJ*, 124, 2364, doi: [10.1086/344069](https://doi.org/10.1086/344069)
- Jiang, L., Fan, X., Ivezić, Ž., et al. 2007, *ApJ*, 656, 680, doi: [10.1086/510831](https://doi.org/10.1086/510831)
- Kadota, K., Sekiguchi, T., & Tashiro, H. 2021, *PhRvD*, 103, 023521, doi: [10.1103/PhysRevD.103.023521](https://doi.org/10.1103/PhysRevD.103.023521)
- Keller, P. M., Thyagarajan, N., Kumar, A., Kanekar, N., & Bernardi, G. 2024, *MNRAS*, 528, 5692, doi: [10.1093/mnras/stae418](https://doi.org/10.1093/mnras/stae418)
- Kondapally, R., Best, P. N., Cochrane, R. K., et al. 2022, *MNRAS*, 513, 3742, doi: [10.1093/mnras/stac1128](https://doi.org/10.1093/mnras/stac1128)
- Koopmans, L., Pritchard, J., Mellema, G., et al. 2015, in *Advancing Astrophysics with the Square Kilometre Array (AASKA14)*, 1, doi: [10.22323/1.215.0001](https://doi.org/10.22323/1.215.0001)
- Lambrides, E., Chiaberge, M., Long, A. S., et al. 2024, *ApJL*, 961, L25, doi: [10.3847/2041-8213/ad11ee](https://doi.org/10.3847/2041-8213/ad11ee)
- Li, W., Inayoshi, K., Onoue, M., & Toyouchi, D. 2023, *ApJ*, 950, 85, doi: [10.3847/1538-4357/acbbbe](https://doi.org/10.3847/1538-4357/acbbbe)
- Liu, Y., Wang, R., Momjian, E., et al. 2021, *ApJ*, 908, 124, doi: [10.3847/1538-4357/abd3a8](https://doi.org/10.3847/1538-4357/abd3a8)
- Lupi, A., Quadri, G., Volonteri, M., Colpi, M., & Regan, J. A. 2023, arXiv e-prints, arXiv:2312.08422, doi: [10.48550/arXiv.2312.08422](https://doi.org/10.48550/arXiv.2312.08422)
- Matsuoka, Y., Strauss, M. A., Kashikawa, N., et al. 2018, *ApJ*, 869, 150, doi: [10.3847/1538-4357/aace7a](https://doi.org/10.3847/1538-4357/aace7a)
- Matsuoka, Y., Onoue, M., Iwasawa, K., et al. 2023, *ApJL*, 949, L42, doi: [10.3847/2041-8213/acd69f](https://doi.org/10.3847/2041-8213/acd69f)
- McGreer, I. D., Becker, R. H., Helfand, D. J., & White, R. L. 2006, *ApJ*, 652, 157, doi: [10.1086/507767](https://doi.org/10.1086/507767)
- Momjian, E., Carilli, C. L., Walter, F., & Venemans, B. 2014, *AJ*, 147, 6, doi: [10.1088/0004-6256/147/1/6](https://doi.org/10.1088/0004-6256/147/1/6)
- Monsalve, R. A., Altamirano, C., Bidula, V., et al. 2024, *MNRAS*, 530, 4125, doi: [10.1093/mnras/stae1138](https://doi.org/10.1093/mnras/stae1138)
- Morales, M. F., & Wyithe, J. S. B. 2010, *ARA&A*, 48, 127, doi: [10.1146/annurev-astro-081309-130936](https://doi.org/10.1146/annurev-astro-081309-130936)
- Morey, K. A., Eilers, A.-C., Davies, F. B., Hennawi, J. F., & Simcoe, R. A. 2021, *ApJ*, 921, 88, doi: [10.3847/1538-4357/ac1c70](https://doi.org/10.3847/1538-4357/ac1c70)
- Munshi, S., Mertens, F. G., Koopmans, L. V. E., et al. 2024, *A&A*, 681, A62, doi: [10.1051/0004-6361/202348329](https://doi.org/10.1051/0004-6361/202348329)
- Navros, O. 2022, PhD thesis, Carnegie Mellon U. (main), doi: [10.1184/R1/19108616.v1](https://doi.org/10.1184/R1/19108616.v1)

- Pacucci, F., Ferrara, A., Volonteri, M., & Dubus, G. 2015, *MNRAS*, 454, 3771, doi: [10.1093/mnras/stv2196](https://doi.org/10.1093/mnras/stv2196)
- Parsons, A. R., Backer, D. C., Foster, G. S., et al. 2010, *AJ*, 139, 1468, doi: [10.1088/0004-6256/139/4/1468](https://doi.org/10.1088/0004-6256/139/4/1468)
- Patil, A. H., Yatawatta, S., Koopmans, L. V. E., et al. 2017, *ApJ*, 838, 65, doi: [10.3847/1538-4357/aa63e7](https://doi.org/10.3847/1538-4357/aa63e7)
- Philip, L., Abdurashidova, Z., Chiang, H. C., et al. 2019, *JAI*, 8, 1950004, doi: [10.1142/S2251171719500041](https://doi.org/10.1142/S2251171719500041)
- Planck Collaboration, Aghanim, N., Akrami, Y., et al. 2020, *A&A*, 641, A6, doi: [10.1051/0004-6361/201833910](https://doi.org/10.1051/0004-6361/201833910)
- Price, D. C., Greenhill, L. J., Fialkov, A., et al. 2018, *MNRAS*, 478, 4193, doi: [10.1093/mnras/sty1244](https://doi.org/10.1093/mnras/sty1244)
- Pritchard, J. R., & Loeb, A. 2012, *RPPH*, 75, 086901, doi: [10.1088/0034-4885/75/8/086901](https://doi.org/10.1088/0034-4885/75/8/086901)
- Runnoe, J. C., Brotherton, M. S., & Shang, Z. 2012, *MNRAS*, 422, 478, doi: [10.1111/j.1365-2966.2012.20620.x](https://doi.org/10.1111/j.1365-2966.2012.20620.x)
- Sabater, J., Best, P. N., Tasse, C., et al. 2021, *A&A*, 648, A2, doi: [10.1051/0004-6361/202038828](https://doi.org/10.1051/0004-6361/202038828)
- Sathyanarayana Rao, M., Singh, S., K. S., S., et al. 2023, *ExA*, 56, 741, doi: [10.1007/s10686-023-09909-5](https://doi.org/10.1007/s10686-023-09909-5)
- Schmidt, M. 1968, *ApJ*, 151, 393, doi: [10.1086/149446](https://doi.org/10.1086/149446)
- Shang, Z., Brotherton, M. S., Wills, B. J., et al. 2011, *ApJS*, 196, 2, doi: [10.1088/0067-0049/196/1/2](https://doi.org/10.1088/0067-0049/196/1/2)
- Shao, Y., Xu, Y., Wang, Y., et al. 2023, *Nature Astronomy*, 7, 1116, doi: [10.1038/s41550-023-02024-7](https://doi.org/10.1038/s41550-023-02024-7)
- Sheth, R. K., & Tormen, G. 2002, *MNRAS*, 329, 61, doi: [10.1046/j.1365-8711.2002.04950.x](https://doi.org/10.1046/j.1365-8711.2002.04950.x)
- Shimabukuro, H., Ichiki, K., Inoue, S., & Yokoyama, S. 2014, *PhRvD*, 90, 083003, doi: [10.1103/PhysRevD.90.083003](https://doi.org/10.1103/PhysRevD.90.083003)
- Shimabukuro, H., Ichiki, K., & Kadota, K. 2020, *PhRvD*, 101, 043516, doi: [10.1103/PhysRevD.101.043516](https://doi.org/10.1103/PhysRevD.101.043516)
- Shimasaku, K., & Izumi, T. 2019, *ApJL*, 872, L29, doi: [10.3847/2041-8213/ab053f](https://doi.org/10.3847/2041-8213/ab053f)
- Silk, J., & Rees, M. J. 1998, *A&A*, 331, L1, doi: [10.48550/arXiv.astro-ph/9801013](https://doi.org/10.48550/arXiv.astro-ph/9801013)
- Singh, S., Subrahmanyam, R., Udaya Shankar, N., et al. 2018, *ApJ*, 858, 54, doi: [10.3847/1538-4357/aabae1](https://doi.org/10.3847/1538-4357/aabae1)
- Square Kilometre Array Cosmology Science Working Group, Bacon, D. J., Battye, R. A., et al. 2020, *PASA*, 37, e007, doi: [10.1017/pasa.2019.51](https://doi.org/10.1017/pasa.2019.51)
- Stern, D., Djorgovski, S. G., Perley, R. A., de Carvalho, R. R., & Wall, J. V. 2000, *AJ*, 119, 1526, doi: [10.1086/301316](https://doi.org/10.1086/301316)
- Sun, T.-Y., Shao, Y., Li, Y., Xu, Y., & Zhang, X. 2024, *arXiv e-prints*, arXiv:2407.14298, doi: [10.48550/arXiv.2407.14298](https://doi.org/10.48550/arXiv.2407.14298)
- Thompson, A. R., Moran, J. M., & Swenson, George W., J. 2017, *Interferometry and Synthesis in Radio Astronomy*, 3rd Edition, doi: [10.1007/978-3-319-44431-4](https://doi.org/10.1007/978-3-319-44431-4)
- Tingay, S. J., Goeke, R., Bowman, J. D., et al. 2013, *PASA*, 30, e007, doi: [10.1017/pasa.2012.007](https://doi.org/10.1017/pasa.2012.007)
- van Haarlem, M. P., Wise, M. W., Gunst, A. W., et al. 2013, *A&A*, 556, A2, doi: [10.1051/0004-6361/201220873](https://doi.org/10.1051/0004-6361/201220873)
- Šoltinský, T., Bolton, J. S., Molero, M., et al. 2023, *MNRAS*, 519, 3027, doi: [10.1093/mnras/stac3710](https://doi.org/10.1093/mnras/stac3710)
- Šoltinský, T., Bolton, J. S., Hatch, N., et al. 2021, *MNRAS*, 506, 5818, doi: [10.1093/mnras/stab1830](https://doi.org/10.1093/mnras/stab1830)
- Wang, F., Yang, J., Fan, X., et al. 2021, *ApJL*, 907, L1, doi: [10.3847/2041-8213/abd8c6](https://doi.org/10.3847/2041-8213/abd8c6)
- Wang, R., Carilli, C. L., Beelen, A., et al. 2007, *AJ*, 134, 617, doi: [10.1086/518867](https://doi.org/10.1086/518867)
- Willott, C. J., Delorme, P., Reylé, C., et al. 2010, *AJ*, 139, 906, doi: [10.1088/0004-6256/139/3/906](https://doi.org/10.1088/0004-6256/139/3/906)
- Wyithe, J. S. B., & Loeb, A. 2003, *ApJ*, 595, 614, doi: [10.1086/377475](https://doi.org/10.1086/377475)
- Xu, Y., Chen, X., Fan, Z., Trac, H., & Cen, R. 2009, *ApJ*, 704, 1396, doi: [10.1088/0004-637X/704/2/1396](https://doi.org/10.1088/0004-637X/704/2/1396)
- Xu, Y., Ferrara, A., & Chen, X. 2011, *MNRAS*, 410, 2025, doi: [10.1111/j.1365-2966.2010.17579.x](https://doi.org/10.1111/j.1365-2966.2010.17579.x)
- Xu, Y., Ferrara, A., Kitaura, F. S., & Chen, X. 2010, *Science China Physics, Mechanics, and Astronomy*, 53, 1124, doi: [10.1007/s11433-010-3208-x](https://doi.org/10.1007/s11433-010-3208-x)
- Xu, Y., & Zhang, X. 2020, *SCPMA*, 63, 270431, doi: [10.1007/s11433-020-1544-3](https://doi.org/10.1007/s11433-020-1544-3)
- Yang, J., Wang, F., Fan, X., et al. 2021, *ApJ*, 923, 262, doi: [10.3847/1538-4357/ac2b32](https://doi.org/10.3847/1538-4357/ac2b32)
- Zubovas, K., & King, A. 2021, *MNRAS*, 501, 4289, doi: [10.1093/mnras/stab004](https://doi.org/10.1093/mnras/stab004)